Brain Structure and Function (2023) 228:1885–1899
https://doi.org/10.1007/s00429-023-02683-2

ORIGINAL ARTICLE

Morphometric analysis of medial temporal lobe subregions in Alzheimer's disease using high-resolution MRI

Emre Hari[1,2,3] · Elif Kurt[2,3] · Cigdem Ulasoglu-Yildiz[2,3] · Ali Bayram[2,3] · Başar Bilgic[4] · Tamer Demiralp[2,5] · Hakan Gurvit[4]

Received: 16 January 2023 / Accepted: 7 July 2023 / Published online: 24 July 2023
© The Author(s), under exclusive licence to Springer-Verlag GmbH Germany, part of Springer Nature 2023

Abstract

The spread pattern of progressive degeneration seen in Alzheimer's disease (AD) to small-scale medial temporal lobe subregions is critical for early diagnosis. In this context, it was aimed to examine the morphometric changes of the hippocampal subfields, amygdala nuclei, entorhinal cortex (ERC), and parahippocampal cortex (PHC) using MRI. MRI data of patients diagnosed with 20 Alzheimer's disease dementia (ADD), 30 amnestic mild cognitive impairment (aMCI), and 30 subjective cognitive impairment (SCI) without demographic differences were used. Segmentation and parcellation were performed using FreeSurfer. The segmentation process obtained volume values of 12 hippocampal subfields and 9 amygdala nuclei. Thickness values of ERC and PHC were calculated with the parcellation process. ANCOVA was performed using age, education and gender as covariates to evaluate the intergroup differences. Linear discriminant analysis was used to investigate whether atrophy predicted groups at an early stage. ERC and PHC thickness decreased significantly throughout the disease continuum, while only ERC was affected in the early stage. When the hippocampal and amygdala subfields were compared volumetrically, significant differences were found in the amygdala between the SCI and aMCI groups. In the early period, only volume reduction in the anterior amygdaloid area of the amygdala nuclei exceeded the significance threshold. Research on AD primarily focuses on original hippocampocentric structures and their main function which is episodic memory. Our results emphasized the significance of so far relatively neglected olfactocentric structures and their functions, such as smell and social cognition in the pre-dementia stages of the AD process.

Keywords Alzheimer's disease · Magnetic resonance imaging · Hippocampal subfields · Amygdala nuclei · Morphometric analysis

✉ Emre Hari
emrehr@hotmail.com

Elif Kurt
elifkurt@istanbul.edu.tr

Cigdem Ulasoglu-Yildiz
cigdemulasoglu@gmail.com

Ali Bayram
ali.bayram@istanbul.edu.tr

Başar Bilgic
bbilgic@istanbul.edu.tr

Tamer Demiralp
demiralp@istanbul.edu.tr

Hakan Gurvit
gurvit@istanbul.edu.tr

[1] Graduate School of Health Sciences, Istanbul University, Bozdogan Kemeri Caddesi No:8 Vezneciler Hamami Sokagi, Vezneciler, 34216 Fatih, Istanbul, Turkey

[2] Hulusi Behcet Life Sciences Research Laboratory, Neuroimaging Unit, Istanbul University, 34093 Istanbul, Turkey

[3] Department of Neuroscience, Aziz Sancar Institute of Experimental Medicine, Istanbul University, 34093 Istanbul, Turkey

[4] Department of Neurology, Behavioral Neurology and Movement Disorders Unit, Istanbul Faculty of Medicine, Istanbul University, 34093 Istanbul, Turkey

[5] Department of Physiology, Istanbul Faculty of Medicine, Istanbul University, 34093 Istanbul, Turkey

Introduction

Alzheimer's disease (AD) is a neurodegenerative disease that causes progressive cognitive impairment. The disease continuum is divided into preclinical AD, AD-related mild cognitive impairment (AD-MCI), and AD dementia (ADD) stages (Molinuevo et al. 2017). Subjective cognitive impairment (SCI) is a more recent term that defines individuals classified in the preclinical stage with neuropsychological test performance within the normative range but have self-reported complaints in their cognitive capacities (Jessen et al. 2014). MCI is considered the predementia stage of the disease. This syndrome is characterized by objective memory deficits, and there is a high risk of progression to dementia. Such clinical symptoms are presumably caused by synaptic and neuronal losses that lead to structural changes quantifiable by volumetric imaging methods (DeTure & Dickson 2019). When patients are diagnosed with dementia, these changes in the brain are widespread and advanced. For this reason, it has become essential to examine the patterns of change in the preclinical stages of the disease by using neuroimaging methods for the early diagnosis of AD.

Deposition of amyloid-beta (Aβ) plaques in the neural parenchyma and neurofibrillary tangles (NFTs) consisting of hyperphosphorylated tau protein within the neurons are the main neuropathological changes in AD (Sanabria-Castro et al. 2017). These depositions in AD occur in succession (NFTs following plaques) long before the first symptoms appear (Roberts et al. 2008). The first neuropathological changes related to typical tau protein accumulation and spread, which are associated with clinical symptoms, start from the pyramidal neurons located in the second layer of the entorhinal cortex (ERC) and spread trans-synaptically to other medial temporal lobe structures (Braak and Braak 1995). This propagation pattern induces progressive episodic memory impairment, which is the earliest symptom of the typical presentation and is reflected in the clinic, primarily in the form of an inability to cope with novel stimuli and compensate for this failure with familiarity (C. R. J. Jack et al. 2010; Wilson et al. 2006). The medial temporal lobe encompasses a number of different anatomical structures, primarily the parahippocampal cortex, ERC and perirhinal cortex (PRC) as well as the hippocampal formation and amygdala (Squire et al. 2004). Therefore, it is essential in the early diagnosis of AD to quantify the atrophy in medial temporal lobe structures with volumetric methods or visual assessment scales (Jack et al. 2011; Scheltens et al. 1992).

The hippocampal formation and amygdala are not homogeneous structures but possess different subsectors and nuclei with distinct cytoarchitectony, functions, and connections (Mai and Paxinos 2011; van Strien et al. 2009). The hippocampal formation is neuroanatomically subdivided into subiculum (SUB), cornu ammonis (CA1, CA2, CA3, and CA4 subsectors), and dentate gyrus (Mai and Paxinos 2011; Schultz and Engelhardt 2014; Strien et al. 2009). When evaluated functionally, the dentate gyrus is known for its role in pattern separation, CA3 in pattern completion, CA1 in integrating inputs, and SUB in recall (Small et al. 2011). The amygdala, composed of a group of nuclei, is another part of the medial temporal lobe, which controls attention, motivation, learning, and memory, particularly emotional conditioning, autonomic and olfactory functions. Its anterior part is surrounded by the piriform cortex and entorhinal sulcus, and its ventral part is by the ERC. Yılmazer-Hanke 2012 divided the amygdala into two cortex-like input sectors and one output sector that does not resemble the cortex due to the lack of laminarization seen in the cortex-like sectors (Yilmazer-Hanke 2012). The first input sector is the superficial cortex-like region (sCLR), also called the olfactory amygdala, which receives direct input from the olfactory bulb through the lateral olfactory tract. The other input sector, the basolateral nuclear group, is crucial in maintaining attention and alertness. The third sector, the centromedial group, is the center of the outputs of sCLR and basolateral nuclear group and mediates autonomic responses.

Since the amygdala consists of small-sized nuclei, it has generally been considered as a whole in research. Recent developments in neuroimaging methods enabled the differentiation of its nuclei. Nine amygdala nuclei have been classified in an amygdala atlas created by Saygın et al. 2017 using in vivo magnetic resonance imaging (MRI) data: anterior amygdaloid area (AAA), cortico-amygdaloid transition area (CAT), and cortical nucleus (Co) correspond to the sCLR sector; lateral nucleus (La), basal nucleus (Ba), paralaminar nucleus (PL), and accessory basal nucleus (AB) correspond to the basolateral nuclear group sector, and finally the medial nucleus (Me) and the central nucleus (Ce) to the centromedial group sector of Yılmazer-Hanke (Saygin et al. 2017; Yilmazer-Hanke 2012).

One of the most important reasons why the propagation pattern of NFTs in medial temporal lobe structures could not be widely documented in in-vivo neuroimaging studies is that the automatic hippocampal and amygdala segmentation was not detailed enough until recently. It is currently possible to segment the hippocampal subfields and amygdala nuclei and calculate the volumes of these structures reliably by using advanced segmentation methods. This study aimed to investigate the susceptibility of ERC, parahippocampal cortex, hippocampal subfields, and amygdala nuclei to progressive neurodegeneration along the Alzheimer's disease using an automatic segmentation and parcellation tool for anatomic MRI data. For this purpose, individual cortical

thickness and subcortical volumetric values obtained using advanced automatic parcellation and segmentation methods for structural MRI data were compared between groups.

Materials and methods

Participants

The study included 20 participants diagnosed with mild ADD, 30 with amnestic MCI (aMCI), and 30 with SCI who were followed up in the Department of Neurology, Behavioral Neurology and Movement Disorders Unit of Istanbul University, Istanbul Faculty of Medicine. Clinical Dementia Rating (CDR), Mini-Mental State Examination (MMSE), and Free and Cued Selective Reminding Test (FCSRT) scores were used for inclusion criteria (Buschke 1984; Folstein et al. 1975; Ivnik et al. 1997; Morris 1991). Based on the National Institute on Aging-Alzheimer's Association (NIA-AA) criteria, the ADD group consisted of individuals diagnosed with early-stage typical ADD with a CDR score of 0.5 or 1 and no other neuropsychiatric diagnosis other than dementia (McKhann et al. 2011). The aMCI group consisted of patients diagnosed with aMCI according to the Petersen criteria, had a CDR score of 0.5 and FCSRT-total free recall (TFR) score of less than or equal to 24, and had no other neuropsychiatric diagnosis (Grober et al. 2010; Petersen 2004). The SCI group consisted of subjects with subjective memory complaints with a CDR score of 0 and an FCSRT-TFR score of higher than 24 (Jessen et al. 2014). If there were any uncertainty about the diagnosis, a detailed clinical examination was supplemented by an examination of the cerebrospinal fluid for AD biomarkers.

MRI acquisition

The structural MRI images were acquired at Hulusi Behcet Life Sciences Research Laboratory, Istanbul University, using a 3 Tesla magnetic resonance imaging system (Phillips, Achieva, Best, The Netherlands) equipped with a 32-channel SENSE head coil. T1-weighted structural images were recorded with 3D TFE (Turbo Field Echo) sequence in the axial plane (aligned with the anterior commissure-posterior commissure line) with the following parameters: Total scan time: 5 min 55 s, time of repetition/time of echo: 8.3/3.8 ms, flip angle: 8°, field of view: 220 × 240 mm, matrix: 252 × 227, 180 axial slices (with no gap), reconstructed to 1 mm^3 isotropic voxels.

MRI analysis

Subcortical segmentation and cortical parcellation of structural MRI data were performed using FreeSurfer (https://surfer.nmr.mgh.harvard.edu, version Dev 6.0.0). Firstly, FreeSurfer standard *recon-all* steps were applied to the individual structural data of all participants (Fischl et al. 2002). After this stage, the skull-stripping, segmentation, and parcellation processes of all participants were controlled with a Freeview viewer. In the next step, detailed segmentation was performed for the hippocampal subfields and the amygdala. Since no single atlas contains detailed sub-areas of the medial temporal lobe structures, three different anatomical atlases available in FreeSurfer were used. For hippocampal subfields, the hippocampal formation atlas created by Iglesias and coworkers using high-resolution MRI data was used, and volume values were calculated for each participant (Iglesias et al. 2015). Subjects' hippocampal formation was divided into 12 hippocampal subfields, namely parasubiculum, presubiculum, SUB, CA1, CA3 (includes CA2), CA4, dentate gyrus, molecular layer, hippocampal amygdaloid transition area, fimbria, hippocampal tail, and hippocampal fissure (Iglesias et al. 2015). For the segmentation of amygdala nuclei, the atlas by Saygın et al. 2017 was used (Saygin et al. 2017), and volume values were obtained for the AAA, CAT, La, Ba, PL, AB, Me, Ce and Co (Saygin et al. 2017). Subcortical structures in the amygdala and hippocampal atlases are shown in three dimensions in Fig. 1A, B. Volume values were normalized using estimated total intracranial volume (eTIV) to correct for the effects of participants' brain sizes.

Cortical thickness values were measured by calculating the shortest distance between the pial surface and white matter at each cortical vertex (Dale et al. 1999). Then, the individuals' reconstructed brains were projected to a spherical space to match the cortical geometry between subjects, and the cortical thickness maps were spatially smoothed with a Gaussian kernel (10 mm full-width at half-maximum). Finally, the group comparisons are carried out on the cortical thickness values within the ERC and parahippocampal cortex parcels of the Desikan-Killiany atlas (Desikan et al. 2006). The 2 parcels in the Desikan-Killiany atlas are shown in Fig. 1C.

Statistical analysis

Statistical analyses of the normalized amygdala and hippocampal volume values obtained from the three groups were performed with the SPSS (IBM SPSS Statistics version 26, https://www.ibm.com/tr-tr/products/spss-statistics) statistical program. For group comparisons, analysis of covariance (ANCOVA) was applied by controlling the effect of age, education, and gender. First, total hippocampus and amygdala volumes were compared. After Bonferroni correction the significance threshold was set at $p < 0.0041$ (2 structures × 2 hemispheres × 3 groups). Detailed analyzes of the amygdala and hippocampal subfields were performed

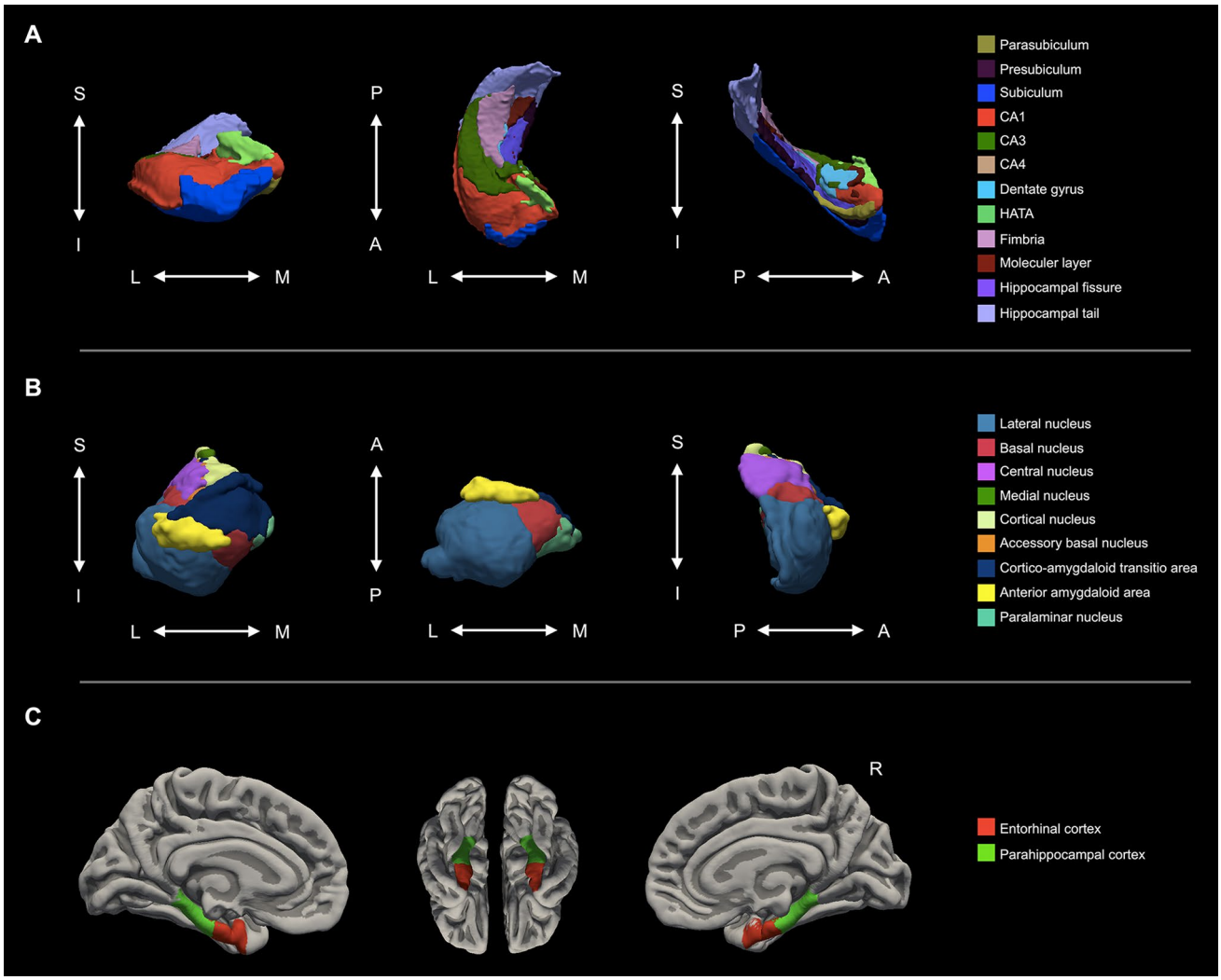


Fig. 1 3D representation of the anatomical structures in the atlases used in the research. **A** Subfields in the hippocampal formation atlas, **B** subfields in the amygdala atlas, **C** cortical areas selected from the Desikan-Killiany atlas. *HATA* Hippocampal-Amygdaloid Transition Area; *CA* Cornu Ammonis; *I* Inferior; *S*: Superior; *A* Anterior; *P* Posterior; *R* Right

by correcting for the multiple comparisons for the 21 bilateral anatomical structures with a threshold of $p < 0.0003$ (21 structures × 2 hemispheres × 3 groups).

Cortical thickness values of the three groups were compared with the general linear model by controlling the effects of age, education, and gender, and then post hoc analyses were performed. Monte Carlo simulation cluster analysis with 10000 iterations was used for multiple comparison correction (cluster-forming threshold: $p < 0.01$; cluster-wise threshold: $p < 0.01$).

Pearson correlation analyses were performed to evaluate the relationship between the volume and cortical thickness values affected in the early stages of the disease (SCI vs aMCI) and the memory scores. The performance of the same variables in discriminating the groups in the AD continuum was additionally tested using stepwise linear discriminant analysis with cross-validation between pairs of disease stages by including each of the variables and age, education and gender in the model. Since three linear discriminant analyzes were performed (ADD vs. aMCI, ADD vs. SCI, and aMCI vs. SCI), the threshold for significance was set to $p < 0.017$ (0.05/3 discriminant function analyzes).

Shapiro–Wilk test was first applied for demographic and clinical data, and the data distribution was examined. In analyzing normally distributed data, one-way analysis of variance (ANOVA) and post hoc comparisons were performed using Bonferroni correction. Kruskal–Wallis H test was used to analyze data that was not normally distributed. In post hoc analyzes, the Mann–Whitney U test was performed, and Bonferroni correction was applied for multiple comparisons. The Chi-square test was performed to examine the gender distribution between the groups.

Results

Demographic and clinical results

The statistical analysis results of the demographic and clinical data are shown in Table 1. No significant difference was found between the groups in terms of age, education and gender ratio, respectively ($\chi^2 = 3.209$, $p = 0.201$; $\chi^2 = 1.647$, $p = 0.439$; $\chi^2 = 4.469$, $p = 0.107$).

Analysis of clinical data showed a statistically significant difference between the groups in terms of MMSE ($\chi^2 = 36.122$, $p < 0.001$) and FCSRT-TFR scores ($F(2,79) = 111.984$, $p < 0.001$). Post hoc analyzes of clinical data showed significant differences among all clinical groups.

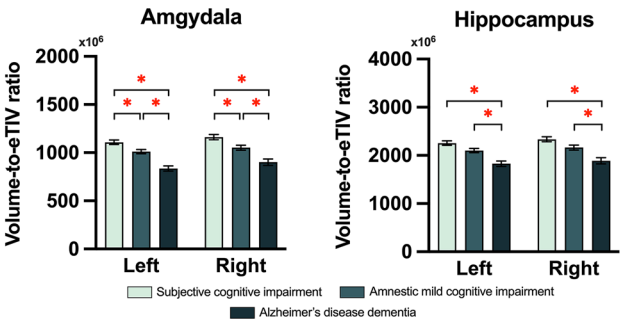


Fig. 2 Post hoc comparisons of the total amygdala and hippocampus volumes between pairs of clinical groups. Mean amygdala and hippocampus volumes to eTIV ratios have been reported. The effects of age, education, and gender were controlled. The statistical results were Bonferroni corrected (2 structures × 2 hemispheres × 3 groups) by setting the significance threshold at $^*p < 0.0041$

Subcortical volume results

The ANCOVA analysis conducted on the total volumes of amygdala (Right: $F(2,74) = 15.781$ $p = 1.50\text{E-}06$; Left: $F(2,74) = 25.579$ $p = 7.00\text{E-}07$) and hippocampus (Right: $F(2,74) = 11.670$ $p = 8.55\text{E-}07$; Left: $F(2,74) = 16.976$ $p = 6.50\text{E-}06$) normalized by the eTIV revealed significant between-group differences in each hemisphere. Post hoc analyses of the total amygdala and hippocampus volume differences between pairs of clinical groups are shown in Fig. 2.

Tables 2 and 3 report the significant volume differences for the amygdala nuclei and hippocampal subfields among the three clinical groups, while Figs. 3 and 4 display the post hoc comparisons of them between pairs of groups. Post hoc comparisons of the volumes of the amygdala nuclei between pairs of clinical groups were performed on the bilateral La, Ba, AB, AAA, PL, CAT, Co, and left Ce, which revealed significant results in the ANCOVA among the three patient groups. Similarly, post hoc comparisons on the hippocampal subfields were performed only on those, which displayed significant differences in the ANCOVA analysis between the three groups. All post hoc results are Bonferroni-corrected for the total number of the amygdala nuclei + hippocampal subfields (21), hemispheres (2) and number of pair-wise comparisons (3) by setting the significance threshold at $p < 0.0003$.

Entorhinal and parahippocampal cortical thickness results

The ANCOVA of the cortical thickness revealed a significant group effect for the parahippocampal cortex and ERC in both hemispheres (Fig. 5). Post hoc comparisons between pairs of the 3 patient groups showed statistically significant decrease in the thickness for the bilateral ERC and parahippocampal

Table 1 Demographic and clinical results

	Mean ± standard deviation			Post hoc results		
	SCI ($n = 30$)	aMCI ($n = 30$)	ADD ($n = 20$)	SCI vs. ADD	SCI vs. aMCI	aMCI vs. ADD
Age[c]	62.57 ± 7.93	63.90 ± 7.63	67.40 ± 10.19	–	–	–
Gender(F/M)	11 / 19	19 / 11	11 / 9	–	–	–
Education[c]	13.07 ± 4.83	11.20 ± 4.96	11.15 ± 4.54	–	–	–
MMSE[c]	29.03 ± 1.24	27.90 ± 1.69	23.20 ± 3.85	$U = 33.500$ $p < 0.001$	$U = 257.500$ $p < 0.05$	$U = 80.000$ $p < 0.001$
FCSRT-TFR[a]	30.53 ± 4.13	18.23 ± 4.46	8.40 ± 7.34	$p < 0.001$	$p < 0.001$	$p < 0.001$

SCI Subjective cognitive impairment; *aMCI* Amnestic mild cognitive impairment; *ADD* Alzheimer's disease dementia; *F* Female; *M* Male; *MMSE* Mini-Mental State Examination; *FCSRT-TFR* Free and Cued Selective Reminding Test-Total Free Recall

[a]One-way ANOVA

[b]Chi-square

[c]Kruskal-Wallis H test and Mann–Whitney U test for post hoc comparisons using Bonferroni correction; The significance threshold was set as $p < 0.05$

Table 2 ANCOVA results for nuclei of the amygdala

	Volume-to-eTIV ratio ($\times 10^{-6}$)					
	SCI	aMCI	ADD	*F (2,74)*	*p*	η^2
Right						
Total amygdala	1159.138 ± 27.396	1052.359 ± 26.649	901.830 ± 32.845	15.781	**1.50E-06***	0.493
Lateral nucleus	447.645 ± 9.823	410.261 ± 9.555	368.410 ± 11.776	10.020	**1.82E-05***	0.379
Basal nucleus	288.518 ± 7.129	257.957 ± 6.934	219.691 ± 8.547	16.689	**4.00E-07***	0.505
Accessory basal nucleus	173.639 ± 5.139	160.825 ± 4.998	125.692 ± 6.161	18.893	**5.00E-07***	0.537
AAA	38.283 ± 0.966	32.584 ± 0.940	28.399 ± 1.158	15.579	**1.00E-07***	0.516
Central nucleus	31.597 ± 1.552	29.560 ± 1.510	22.599 ± 1.861	7.365	0.002	0.302
Medial nucleus	15.973 ± 0.873	14.056 ± 0.850	11.647 ± 1.047	4.572	0.011	0.222
Cortical nucleus	18.601 ± 0.719	16.959 ± 0.700	13.343 ± 0.862	10.664	**8.39E-05***	0.399
CAT	112.594 ± 3.170	101.493 ± 3.084	87.085 ± 3.800	13.173	**1.94E-05***	0.483
Paralaminar nucleus	32.290 ± 0.818	28.664 ± 0.796	24.964 ± 0.981	14.425	**2.10E-06***	0.453
Left						
Total amygdala	1105.500 ± 23.327	1010.474 ± 22.691	835.749 ± 27.967	25.579	**7.00E-07***	0.594
Lateral nucleus	436.604 ± 9.048	396.598 ± 8.801	346.212 ± 10.847	17.553	**2.00E-07***	0.478
Basal nucleus	274.410 ± 6.216	251.120 ± 6.046	204.600 ± 7.452	24.033	**9.07E-09***	0.579
Accessory basal nucleus	161.047 ± 4.385	151.901 ± 4.265	113.352 ± 5.257	27.552	**1.14E-09***	0.618
AAA	36.053 ± 0.833	30.870 ± 0.811	25.446 ± 0.999	30.076	**2.76E-10***	0.626
Central nucleus	28.879 ± 1.282	25.200 ± 1.247	18.396 ± 1.537	16.066	**1.26E-05***	0.450
Medial nucleus	13.319 ± 0.840	11.892 ± 0.817	9.839 ± 1.007	4.886	0.041	0.238
Cortical nucleus	16.293 ± 0.688	15.664 ± 0.669	11.627 ± 0.825	10.763	**1.09E-04***	0.392
CAT	107.891 ± 2.752	98.485 ± 2.677	81.069 ± 3.300	18.309	**3.00E-07***	0.571
Paralaminar nucleus	31.005 ± 0.775	28.743 ± 0.754	25.207 ± 0.929	9.668	**6.85E-05***	0.371

Values shown are in mean ± standard deviation. ANCOVA was performed by controlling the effect of age, education, and gender (Bonferroni-corrected significance threshold $*p < 0.0003$)

SCI Subjective cognitive impairment; *aMCI* Amnestic mild cognitive impairment; *ADD* Alzheimer's disease dementia; *AAA* Anterior amygdaloid area; *CAT* Cortico-amygdaloid transition area; *eTIV* estimated total intracranial volume

cortex in the ADD group in comparison to both SCI and aMCI groups, while aMCI vs. SCI comparison revealed a significant reduction of only the right ERC thickness in the aMCI group (Fig. 5, Supplementary Material Table S1).

Stepwise linear discriminant analysis results

As a result of the stepwise linear discriminant analysis, among the variables included in the model (ERC, amygdala, AAA, age, education and gender), it was determined that the left amygdala volume [Standardized Canonical Discriminant Function Coefficients (SCDFC) = 1.135] and gender (SCDFC = − 0.651), discriminated between aMCI and ADD groups (Accuracy = 78%, sensitivity = 65%, specificity = 86.7%, Wilks' $\lambda = 0.613$, $\chi^2 = 23.003$, eigenvalue = 0.631, canonical correlation = 0.622, $p = 1.01E\text{-}05$). It was found that the left amygdala volume (SCDFC = 0.988) in the model discriminated the SCI and ADD groups (Accuracy = 90%, sensitivity = 85%, specificity = 93.3%, Wilks' $\lambda = 0.401$, $\chi^2 = 43.396$, eigenvalue = 1.493, canonical correlation = 0.774, $p = 4.47E\text{-}11$). Finally, stepwise linear discrimination analysis showed that left AAA (SCDFC = 0.988) and education (SCDFC = 0.473) discriminated between aMCI and SCI groups (Accuracy = 73.3%, sensitivity = 73.3%, specificity = 73.3%, Wilks' $\lambda = 0.647$, $\chi^2 = 24.806$, eigenvalue = 0.545, canonical correlation = 0.594, $p = 4.11E\text{-}06$).

Correlation analysis results

Correlation analysis was performed between the volumes or thicknesses of the anatomical regions (AAA, total amygdala and ERC), in which a significant difference was detected between the early stages of the disease and FCSRT-TFR scores. Correlation analyses were performed by including all disease groups, and Bonferroni correction was applied for correcting the results of multiple correlation analyses (Statistical significance threshold was set at $p < 0.008$). Bilateral AAA, amygdala volumes and ERC thicknesses displayed significant positive correlations with the FCSRT-TFR scores (Fig. 6), indicating that increased volumes or thicknesses are associated with better recall ability.

Table 3 ANCOVA results for hippocampal subfields

	Volume-to-eTIV ratio ($\times 10^{-6}$)					
	SCI	aMCI	ADD	*F (2,74)*	*p*	η^2
Right						
Total hippocampus	2335.368 ± 53.600	2163.203 ± 52.139	1889.552 ± 64.260	11.670	**8.55E-07***	0.458
Hippocampal tail	361.997 ± 11.631	340.307 ± 11.314	297.387 ± 13.944	4.784	0.003	0.284
Subiculum	296.336 ± 8.050	273.121 ± 7.830	232.076 ± 9.651	10.793	**2.05E-05***	0.418
CA1	443.056 ± 11.399	416.032 ± 11.089	356.564 ± 13.667	9.594	**4.43E-05***	0.399
Hippocampal fissure	126.729 ± 4.508	122.262 ± 4.385	124.551 ± 5.405	0.469	0.786	0.128
Presubiculum	195.856 ± 5.745	177.909 ± 5.588	158.499 ± 6.888	7.504	5.79E-04	0.360
Parasubiculum	39.673 ± 1.691	33.117 ± 1.645	34.917 ± 2.027	3.730	0.027	0.216
Molecular layer	379.147 ± 9.121	352.565 ± 8.872	302.462 ± 10.935	12.424	**7.10E-06***	0.459
Dentate gyrus	201.723 ± 4.875	185.990 ± 4.742	164.041 ± 5.844	11.031	**4.01E-05***	0.438
CA3	152.208 ± 4.400	141.874 ± 4.280	128.001 ± 5.275	5.314	0.004	0.305
CA4	175.940 ± 4.254	163.209 ± 4.138	145.183 ± 5.100	9.192	**1.23E-04***	0.289
Fimbria	49.052 ± 2.118	44.346 ± 2.060	39.084 ± 2.539	4.915	0.017	0.334
HATA	40.381 ± 1.331	34.732 ± 1.295	31.338 ± 1.596	9.723	**2.13E-04***	0.387
Left						
Total hippocampus	2256.090 ± 47.014	2101.148 ± 45.732	1827.886 ± 56.364	16.976	**6.50E-06***	0.574
Hippocampal tail	353.799 ± 11.178	320.483 ± 10.874	273.448 ± 13.402	10.425	**1.35E-04***	0.406
Subiculum	295.763 ± 6.959	276.890 ± 6.769	235.832 ± 8.343	15.953	**3.90E-06***	0.531
CA1	421.940 ± 9.513	400.942 ± 9.253	338.690 ± 11.404	15.534	**2.00E-06***	0.560
Hippocampal fissure	117.357 ± 4.699	116.638 ± 4.571	114.655 ± 5.633	0.016	0.935	0.057
Presubiculum	199.907 ± 5.687	186.801 ± 5.532	171.163 ± 6.818	5.454	0.009	0.379
Parasubiculum	37.922 ± 1.907	32.776 ± 1.855	37.379 ± 2.287	2.134	0.123	0.187
Molecular layer	367.147 ± 7.870	345.440 ± 7.655	295.159 ± 9.435	17.411	**1.00E-06***	0.591
Dentate gyrus	188.003 ± 4.163	175.946 ± 4.050	152.759 ± 4.991	15.081	**6.10E-06***	0.549
CA3	139.675 ± 3.927	130.105 ± 3.820	116.295 ± 4.708	6.658	0.002	0.377
CA4	164.091 ± 3.479	153.855 ± 3.384	134.840 ± 4.171	14.359	**7.20E-06***	0.504
Fimbria	48.846 ± 2.615	43.178 ± 2.543	42.253 ± 3.135	1.797	0.209	0.170
HATA	38.997 ± 1.442	34.732 ± 1.403	30.069 ± 1.729	7.609	0.001	0.432

Values shown are in mean ± standard deviation. ANCOVA was performed by controlling the effect of age, education, and gender (Bonferroni-corrected significance threshold $*p < 0.0003$)

SCI Subjective cognitive impairment; *aMCI* Amnestic mild cognitive impairment; *ADD* Alzheimer's disease dementia; *HATA* hippocampus-amygdala transition area; *CA* Cornu ammonis; *eTIV* estimated total intracranial volume

Discussion

This study compared volume and cortical thickness changes of medial temporal lobe structures of ADD, aMCI, and SCI groups. Volume reduction and cortical thinning were observed along the SCI, aMCI, ADD continuum in almost all medial temporal lobe structures.

Total hippocampal volumes of the ADD group were bilaterally smaller than the other two groups, whereas the difference between the SCI and aMCI groups did not reach significance. However, total amygdala volumes significantly differed not only in the ADD vs. SCI or ADD vs. aMCI comparisons, but were also significantly reduced in the aMCI compared with the SCI group. These findings indicate that amygdala volume may be a potential imaging marker for the early stages of the disease. Furthermore, a statistically significant cortical thinning was detected in bilateral ERC and parahippocampal cortex in the ADD group compared to the other two groups. Similar to the hippocampal volume results SCI and aMCI groups were not significantly different in terms of parahippocampal cortex thickness, but the right ERC thickness was significantly smaller in the aMCI than the SCI group. Therefore, ERC thickness can also be added to the list of early imaging markers.

All 12 hippocampal subfields in each of the two hemispheres showed a progressive volume decrease along the stages of the disease. However, only five subfields, which are SUB, molecular layer, CA1, CA4, and dentate gyrus, displayed statistically significant bilateral volume reductions in the ADD compared with the SCI group. Additionally, the

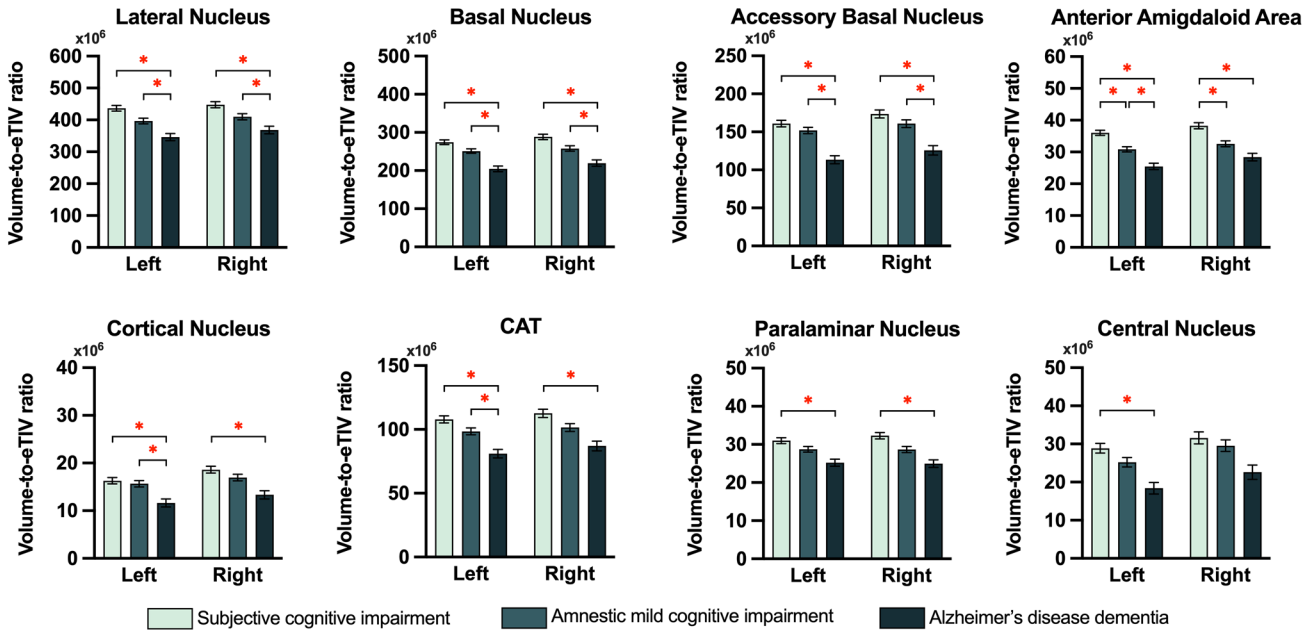


Fig. 3 Post hoc comparisons of the volumes of the amygdala nuclei between pairs of the 3 clinical groups. Mean amygdala nuclei volumes to eTIV ratios have been reported (Bonferroni-corrected significance threshold $*p < 0.0003$). *CAT* Cortico-amygdaloid transition area

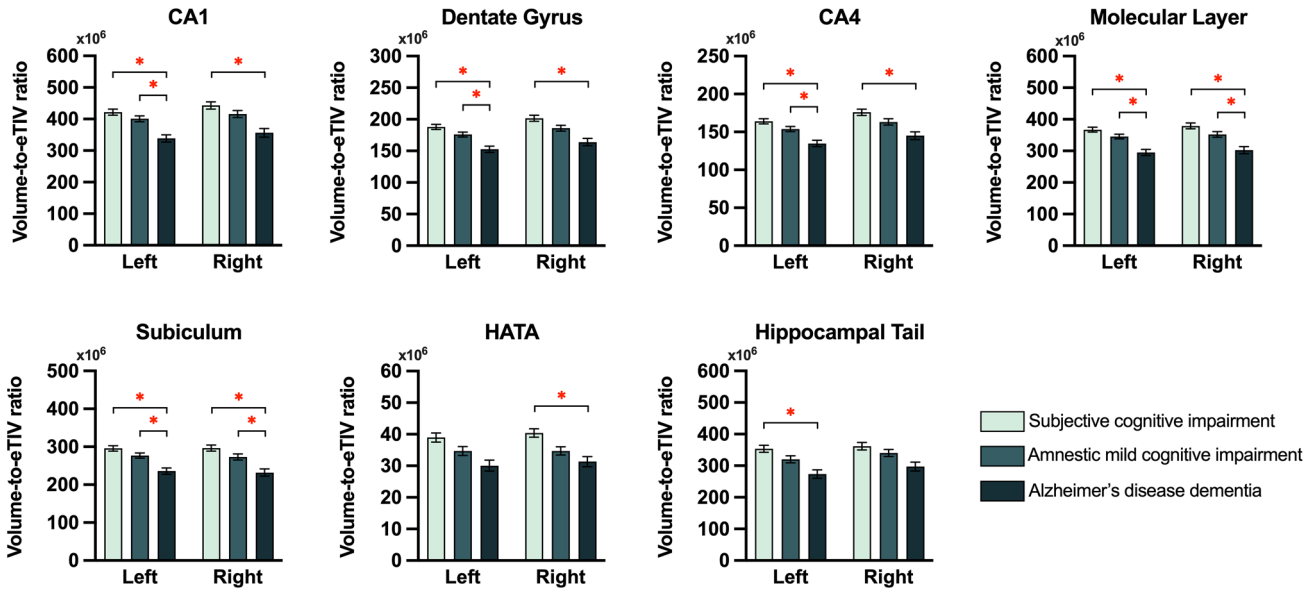


Fig. 4 Post hoc comparisons of hippocampal subfields (Bonferroni-corrected significance threshold $*p < 0.0003$). Mean hippocampal subfield volumes to eTIV ratios have been reported. *HATA* hippocampus-amygdala transition area; *CA* Cornu ammonis

right hippocampal amygdaloid transition area and left hippocampal tail were also significantly smaller in the ADD compared with the SCI group. During the progress from aMCI to ADD, bilateral SUB and molecular layer in addition to the left CA1, CA4 and dentate gyrus showed significant volume reductions. On the other hand, there were no significant volume differences among the groups in bilateral CA3, hippocampal fissures, fimbria, presubiculum, parasubiculum, left hippocampal amygdaloid transition area, and right hippocampal tail. More importantly, we found no volume marker among the hippocampal subfields that would enable early SCI-aMCI differentiation. Yet, SUB, molecular layer, CA1, CA4 and dentate gyrus emerged as consistent markers of advanced AD.

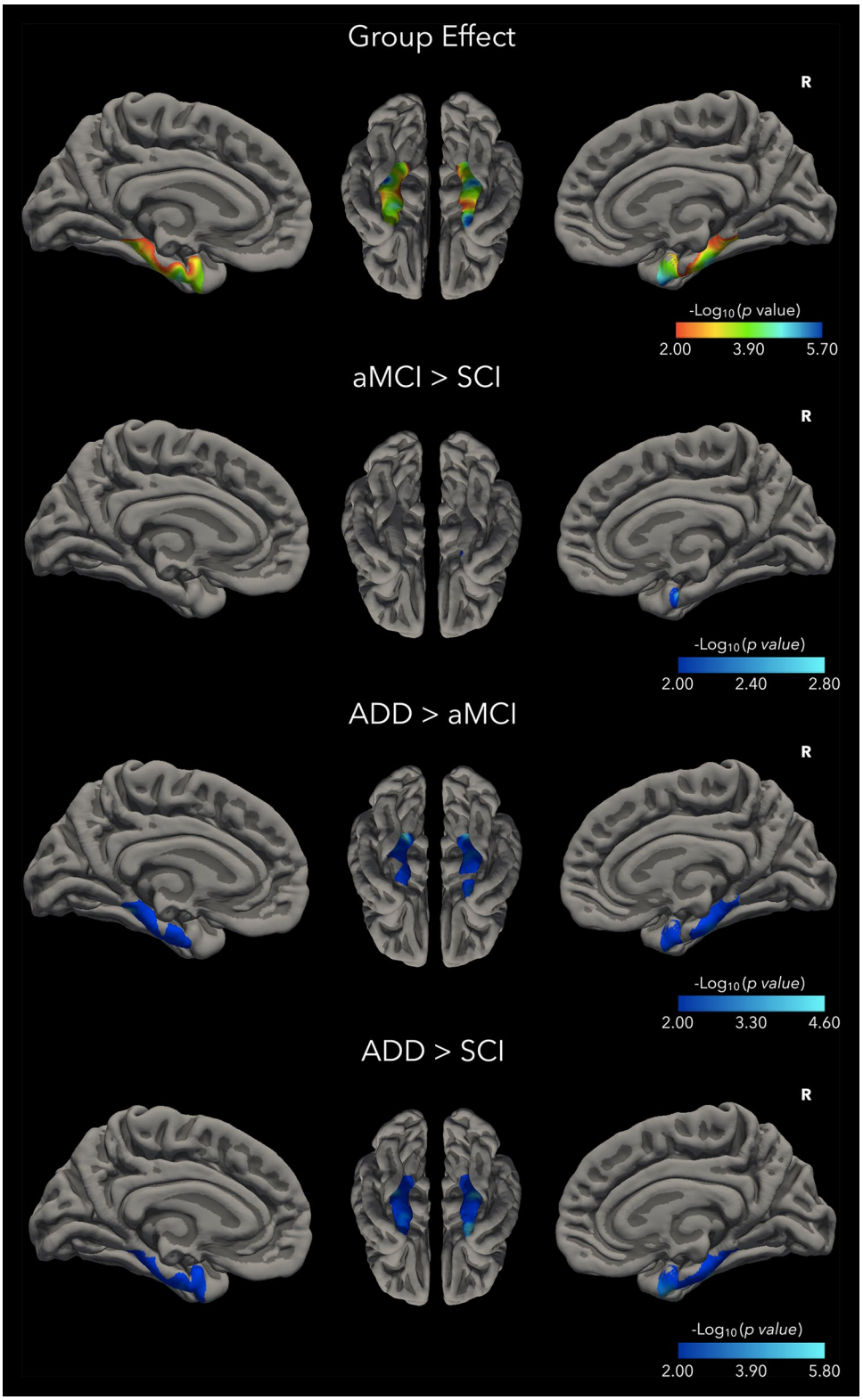


Fig. 5 ANCOVA and post hoc analyzes performed on the entorhinal and parahippocampal cortex thickness values by controlling the effect of age, education, and gender. The significance threshold was set at $p < 0.01$. The color bars display the -log(*p*-value). *SCI* Subjective cognitive impairment; *aMCI* Amnestic mild cognitive impairment; *ADD* Alzheimer's disease dementia; *R* Right

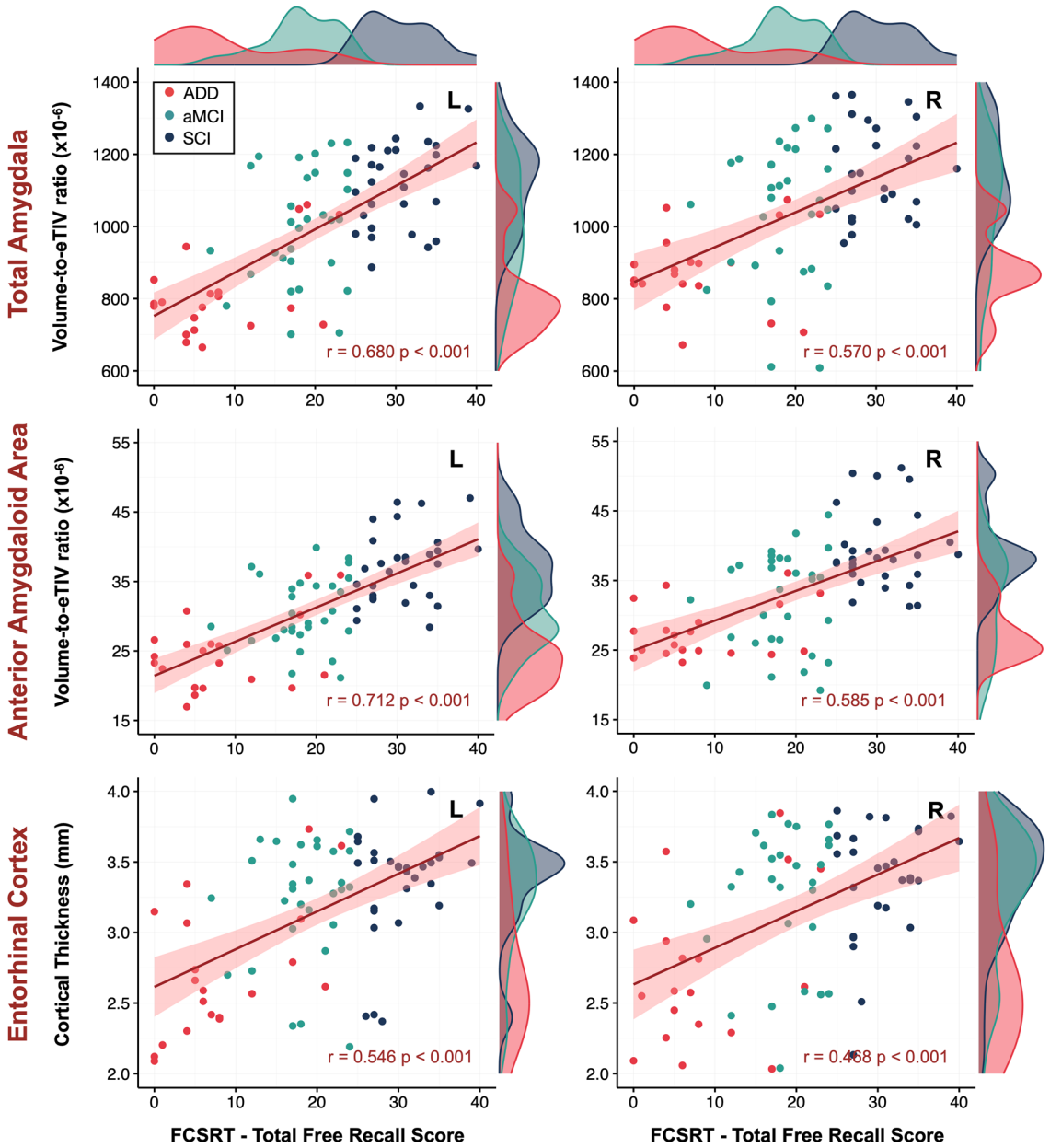


Fig. 6 Pearson correlation analysis results in the anterior amygdaloid area and total amygdala volume to eTIV ratio, and entorhinal cortex thickness with memory scores. *SCI* Subjective cognitive impairment; *aMCI* Amnestic mild cognitive impairment; *ADD* Alzheimer's disease dementia. Bonferroni-corrected significance threshold $p < 0.008$

Among the total 9 amygdala nuclei in each of the two hemispheres, left Ce in addition to seven bilateral nuclei, that are La, Ba, AB, AAA, Co, CAT and PL volumes were significantly smaller in the ADD compared with the SCI group. In the ADD vs. aMCI comparison, bilateral La, Ba and AB in addition to the left AAA, Co and CAT displayed statistically significant volume reductions. No difference was found among the three groups for the bilateral Me and right Ce volumes. The striking finding was the significant bilateral AAA volume reduction in the aMCI compared with the SCI group. This finding promoted the AAA to the previous list of early imaging markers, the total amygdala volume and the ERC thickness. La, Ba, and AB appeared as the more consistent markers of late disease. The linear discriminant analysis results extended the above findings by showing the discriminant power of the left AAA in differentiating SCI from the aMCI group. In addition, the left total amygdala also highly discriminated against the SCI group from both aMCI and ADD. AAA and total amygdala

volumes and the ERC thickness showed also strongly significant correlations with the FCSRT-TFR scores.

Braak and Braak proposed a staging scheme according to deposition quantity and topographical spread pattern of NFTs that defined the Alzheimer's disease continuum (Braak & Braak 1991). In that seminal paper, Braak and Braak graded the quantity of NFTs as follows: (0) with no discernible change, (i) with a few isolated NFTs, (+) with small, (++) moderate, (+++) large numbers of NFTs and finally (g) denotes the presence of ghost tangles. In their staging system, stages I-II is also named as the "transentorhinal," stages III-IV as the "limbic," and V-VI as the "isocortical." Stages I-II correspond to NFT deposits in the transentorhinal cortex (TEC, graded as + to ++) but also in ERC layer II (+), CA1 (i), amygdala (i), basal forebrain (i), and thalamic anterodorsal nucleus (i to +). TEC is part of the Brodmann areas 35 and 36, commonly called the PRC. This spread pattern in stages I-II may partially correspond to SCI, which is included in the preclinical stage of AD (Sperling et al. 2019). During the following limbic stages III-IV, NFTs spread trans-synaptically to hippocampal subfields and involve neighboring limbic and paralimbic regions. In these stages, while NFT accumulation in TEC (+++ to g), ERC (+++), CA1 (++), amygdala (++), and basal forebrain (++) increases, CA4 (+) is added to these anatomical regions. NFT deposits in other hippocampal subfields are either zero or a few isolated. This stage can be conceived as clinically the MCI stage of the disease. In the advanced isocortical stages V-VI, which corresponds clinically to the ADD stage, NFTs spread to the neocortical association areas. At this stage, all hippocampal subfields were affected at a small or moderate grade.

Since TEC was not included in the atlas, we only analyzed ERC thickness and found that it is one of the early affected variables in addition to the total amygdala and AAA volumes. The absence of the TEC thickness value can be considered as one of the limitations of the study since, according to the above statement TEC and ERC are the initial sites of NFT deposition and carry the most severe brunt of this deposition throughout the disease course. Within TEC, BA35 was repeatedly shown as the prime originator of the NFTs. An MRI automatic segmentation study with ADNI data showed that BA35 volume was the only discriminator between preclinical AD (amyloid positive, cognitively unimpaired) and amyloid negative cognitively unimpaired individuals (Wolk et al. 2017). The same group had already shown with automated segmentation methods that BA35 was the area with CA1 to have the most significant differences between the aMCI and cognitively unimpaired groups (Yushkevich et al. 2015). Finally, Yushkevich and colleagues (2021), together with an international collaboration, using 3D, ex vivo imaging with ultra-high field MRI, showed that BA35 NFT burden compared only with ERC, amygdala, anterior CA1 and anterior SUB (Yushkevich et al. 2021).

The right ERC was one of the discriminants of the initial (SCI) and middle (MCI) stages. The finding that the left ERC difference did not reach significance may be due to the relatively small size of study groups, the likely admixture of amyloid positive and negative individuals in both SCI and MCI groups, and the conservative statistical correction methods we used to obtain more precise findings. In line with our findings, a recent study using Alzheimer's disease cohorts reported that the ERC, parahippocampal cortex, and amygdala play a central role in the early appearance of tau (Insel et al. 2023). In studies conducted in independent aging cohorts, it was reported that the amount of tau increased in the medial temporal lobe (entorhinal cortex, parahippocampal gyrus, amygdala), ventral and lateral temporal cortices, precuneus, posterior cingulate and lateral parietal lobes in preclinical AD (Betthauser et al. 2020; Lockhart et al. 2017; Schöll et al. 2016; Sperling et al. 2019; Vemuri et al. 2017).

Our other outperformers deserving to be listed in the early discriminator's list were also extra-hippocampal: both amygdala and their olfactory subnuclei, both AAA. In Braak and Braak's scheme, although the amygdala has a few isolated NFTs in stages I-II, it follows CA1, TEC, and ERC, which show a high accumulation of NFTs throughout the process. In Braak and Braak's scheme, although a few isolated NFTs are observed only in the amygdala at stages I-II, NFT spreading pattern follows CA1, TEC, and ERC with high accumulation throughout the next stages. Amygdala is also listed in Yushkevich et al. (2021) study, as stated above. So, although underappreciated in the literature, amygdala volume decrease throughout the disease course is quite consistent with Braak and Braak's findings more than 30 years ago and with the recent results (Yushkevich et al. 2021). Furthermore, our results suggest that the most consistently affected nucleus of the amygdala, although constituting a relatively small subarea, is the AAA, which is the closest part of the amygdala to the ERC.

In the present study, no hippocampal subfield was different in the SCI-MCI comparison. This may also be due to reasons stated for the left ERC negative finding. On the other hand, despite the statistical power issues, the hippocampal subfields that show a clearly significant volume loss in the later stage of the disease seem to be less sensitive in discriminating the SCI from MCI compared with amygdala and AAA volume. However, SUB, CA1, CA4, and dentate gyrus, which were smaller in the ADD group compared to the earlier stage groups in our study, do not show NFTs accumulation in Stage I-II (Only CA1 Stage II has a small load of NFTs), while NFTs accumulated at a very high level in stage VI. Among our hippocampal subfields that showed no difference among the three groups in the present study that are CA3, pre and para-SUB are still contain numbers

of NFTs in Stage V as listed in Braak and Braak's table. Therefore, our volumetric findings are also generally in line with the original staging. A 2015 review on hippocampal subfield structural imaging with either manual or automatic segmentation in ADD and MCI lists 33 studies published between 2003 and 15 (De Flores et al. 2015). Although different atrophy patterns have been reported for the hippocampal subfields, the most consistent volume reductions were in CA1, SUB, and dentate gyrus, in that order.

One of the early studies showed that more conspicuous amygdala atrophy than the hippocampus can be detected with standard MRI in early-stage ADD patients (Cuénod et al. 1993). In a more recent study with a much larger number of patients with very early (CDR 0.5) and early (CDR 1) stage ADD, atrophy of the amygdala was comparable to atrophy of the hippocampus in each group and was likely to be associated with neuropsychiatric symptoms (Poulin et al. 2011). Postmortem studies have also reported that amygdala atrophy is prominent in AD (Scott et al. 1992). It has been reported that both Aβ plaque and tau NFT pathology in the early stages of the disease also affect the amygdala, similar to the hippocampus (Arriagada et al. 1992; Price et al. 1991; Price and Morris 1999). In a small early study examining the amygdala nuclei, it was reported that although there was a certain volume reduction in all subnuclei, the most prominent cell loss was in Me, Ce, and Co, and the findings were interpreted as the involvement of the oldest structures of the amygdala in terms of morphology, development, and connection (Herzog and Kemper 1980). In a more extensive cohort study, the most prominent NFT and neuritic plaque load were found in AB, Co, and CAT, while the laterobasal nucleus, La, Ce, and Me were relatively preserved; these findings have been interpreted as a predisposition to nuclei that are major targets of hippocampo-amygdalar connectivity (Vogt et al. 1990). Our study found the most consistent volume reductions in La, Ba, AB, and AAA. Parallel to the interpretation of Vogt et al. (1990), it can be argued that due to the reciprocal connections of La, Ba, and AB with ERC and CA1/SUB, AD neuropathological changes cause volume reductions specifically in these nuclei (Vogt et al. 1990). The AAA is one of the primary olfactory cortex structures directly connected to the olfactory bulb via the lateral olfactory tract and is separated from the neighboring ERC by the entorhinal sulcus (Saygin et al. 2017; Yilmazer-Hanke 2012). In many studies investigating the amygdala volumes of Alzheimer's patients at different clinical stages using MRI, it has been reported that there is a continuous decrease in amygdala volumes during the AD continuum, and these decreases are correlated with neuropsychological performance (Beacher et al. 2009; Cherubini et al. 2010; Horínek et al. 2007; Lehmann et al. 2010; Vasconcelos et al. 2011). Amygdala atrophy has been reported even in the preclinical stages of the disease (Fox et al. 1996; Golebiowski et al. 1999; Heun et al. 1997). In addition, it has been suggested by Liu et al. (2010) that amygdala volume is a very important marker for predicting conversion from MCI to ADD (Liu et al. 2010).

Olfactory dysfunction is one of the earliest preclinical symptoms observed in AD (Kotecha et al. 2018). The sense of smell has been reported as a promising early biomarker as it is easy to detect, inexpensive to measure, not dependent on laboratory analysis, and not invasive (Kotecha et al. 2018). Studies investigating olfactory sense in AD emphasize that the sense of smell worsens as the disease progresses and that the dysfunction in the sense of smell has the potential to define AD in the preclinical stages of the disease (Förster et al. 2010; Quarmley et al. 2017; Seligman et al. 2013; Velayudhan et al. 2015; Wang et al. 2010; Ward et al. 2017). Our findings seem to be compatible with the anatomical background of olfactory dysfunction in AD since the AAA is located in the sCLR sector associated with the sense of smell and is affected by the early stages of the disease.

The dual origin hypothesis of the cerebral cortex proposes that allocortical limbic structures eventually reach six layers/isocortical neocortical evolution with two parallel progressive laminarizations. The first is the archicortical hippocampocentric which proceeds with posterior cingulate mesocortical development to dorsal isocortical areas. The second is the paleocortical amygdala-olfactocentric which proceeds with insular-anterior cingulate mesocortical development to ventral isocortical areas (Pandya et al. 2015). These two modes of differentiation also correspond to functional difference. While the archicortical origin moves from memory to other cognitive areas, the paleocortical origin seems to move from smell and emotion to other areas of social cognition (Giaccio 2006). The fact that Alzheimer's disease research focuses on the first origin and neglects the second can be explained by the relative novelty of smell and social cognitive assessment.

Limitations

Although our study includes detailed and rigorous analyses, there are several limitations. The first is that the olfactory senses of the participants were not evaluated. It was thought that only the decrease in AAA volumes in the preclinical stage of the disease, which is one of the interesting findings of the study, may be related to the recently reported olfactory dysfunction in the AD continuum. However, an objective olfactory evaluation of the participants should be made to demonstrate this clearly. In future studies, objectively evaluating olfactory sense and investigating its relationship with volumetric findings may expand the present results. Another limitation of the study could be an average number of participants. However, conservative statistical corrections used

in the study can be considered robust measures to overcome this.

Conclusion

The distinctive patterns of atrophy in the amygdala and hippocampal subfields suggest that pathology in both medial temporal lobe structures may contribute to the characteristic cognitive (memory and social) and perceptual (smell) changes in preclinical AD. The relationship between episodic memory impairment, the earliest sign of the disease, and hippocampocentric structures is well-established. However, the sense of smell and social cognitive changes are relatively neglected in the course of the disease. As a result of this study, it was thought that their evaluation was as important as episodic memory disorder. AAA volume can potentially be an important MRI biomarker for early disease detection. Medial temporal lobe visual rating specifically refers to hippocampal thinning; however, our results suggest that a novel one including the amygdala will be more appropriate.

Supplementary Information The online version contains supplementary material available at https://doi.org/10.1007/s00429-023-02683-2.

Acknowledgements We thank Burak Acar, Elif Yıldırım and Ezgi Soncu Büyükişcan for their contribution. Emre Hari is a PhD scholarship holder from the Council of Higher Education (CoHE) in the field of Human Brain and Neuroscience, which is one of the 100 national priority areas determined by CoHE within the scope of the 100/2000 Program.

Author contributions EH: Conceptualization, Methodology, Formal analysis, Investigation, Writing-original draft, Visualization, Writing-review & editing; EK: Conceptualization, Methodology, Formal analysis, Investigation, Writing-original draft, Visualization, Writing-review & editing; CU-Y: Methodology, Investigation, Formal analysis, Writing-review & editing; AB: Methodology, Investigation, Formal analysis, Writing-review & editing; BB: Methodology, Writing-review & editing, Software, Supervision; TD: Conceptualization, Methodology, Resources, Writing-review & editing, Supervision; HG: Conceptualization, Methodology, Resources, Writing-review & editing, Supervision.

Funding This work was supported by Istanbul University Research Projects Unit (Grant #: 2019K12-149071); Istanbul University Research University Support Program (Grant #: TSA-2022–39128).

Data availability The datasets generated and analyzed during the current study are not publicly available due to ethical reasons but are available from the corresponding author on reasonable request.

Declarations

Conflict of interest The authors declare no competing interests.

Ethical approval The study was approved by the Clinical Research Ethics Committee of Istanbul University, Istanbul Faculty of Medicine. This study was performed in accordance with the ethical principles of the latest version of the Declaration of Helsinki.

Informed consent Written informed consent was provided by all participants.

References

Arriagada PV, Growdon JH, Hedley-Whyte ET, Hyman BT (1992) Neurofibrillary tangles but not senile plaques parallel duration and severity of Alzheimer's disease. Neurology 42(3):631. https://doi.org/10.1212/WNL.42.3.631

Beacher F, Daly E, Simmons A, Prasher V, Morris R, Robinson C, Murphy DGM (2009) Alzheimer's disease and down's syndrome: an in vivo MRI study. Psychol Med 39(4):675–684. https://doi.org/10.1017/S0033291708004054

Betthauser TJ, Koscik RL, Jonaitis EM, Allison SL, Cody KA, Erickson CM, Clark LR (2020) Amyloid and tau imaging biomarkers explain cognitive decline from late middle-age. Brain 143(1):320–335. https://doi.org/10.1093/brain/awz378

Braak H, Braak E (1991) Neuropathological stageing of Alzheimer-related changes. Acta Neuropathol 82(4):239–259. https://doi.org/10.1007/BF00308809

Braak H, Braak E (1995) Staging of Alzheimer's disease-related neurofibrillary changes. Neurobiol Aging 16(3):271–284. https://doi.org/10.1016/0197-4580(95)00021-6

Buschke H (1984) Cued recall in amnesia. J Clin Neuropsychol 6(4):433–440. https://doi.org/10.1080/01688638408401233

Cherubini A, Péran P, Spoletini I, Di Paola M, Di Iulio F, Hagberg GE, Caltagirone C (2010) Combined volumetry and DTI in subcortical structures of mild cognitive impairment and Alzheimer's disease patients. J Alzheimer's Dis 19(4):1273–1282. https://doi.org/10.3233/JAD-2010-091186

Cuénod C-A, Denys A, Michot J-L, Jehenson P, Forette F, Kaplan D, Boller F (1993) Amygdala atrophy in Alzheimer's disease: an in vivo magnetic resonance imaging study. Archiv Neurol 50(9):941–945. https://doi.org/10.1001/archneur.1993.00540090046009

Dale AM, Fischl B, Sereno MI (1999) Cortical surface-based analysis I segmentation and surface reconstruction. Neuroimage 9(2):179–194. https://doi.org/10.1006/nimg.1998.0395

De Flores R, La Joie R, Chételat G (2015) Structural imaging of hippocampal subfields in healthy aging and Alzheimer's disease. Neuroscience 309:29–50. https://doi.org/10.1016/j.neuroscience.2015.08.033

de Vasconcelos LG, Jackowski AP, de Oliveira MO, Flor YMR, Bueno OFA, Brucki SMD (2011) Voxel-based morphometry findings in Alzheimer's disease: neuropsychiatric symptoms and disability correlations-preliminary results. Clinics 66(6):1045–1050. https://doi.org/10.1590/S1807-59322011000600021

Desikan RS, Ségonne F, Fischl B, Quinn BT, Dickerson BC, Blacker D, Hyman BT (2006) An automated labeling system for subdividing the human cerebral cortex on MRI scans into gyral based regions of interest. Neuroimage 31(3):968–980. https://doi.org/10.1016/j.neuroimage.2006.01.021

DeTure MA, Dickson DW (2019) The neuropathological diagnosis of Alzheimer's disease. Mol Neurodegener 14(1):32. https://doi.org/10.1186/s13024-019-0333-5

Fischl B, Salat DH, Busa E, Albert M, Dieterich M, Haselgrove C, Dale AM (2002) Whole brain segmentation: automated

labeling of neuroanatomical structures in the human brain. Neuron 33(3):341–355. https://doi.org/10.1016/s0896-6273(02)00569-x

Folstein MF, Folstein SE, McHugh PR (1975) "Mini-mental state". A practical method for grading the cognitive state of patients for the clinician. J Psychiatric Res 12(3):189–198. https://doi.org/10.1016/0022-3956(75)90026-6

Förster S, Vaitl A, Teipel SJ, Yakushev I, Mustafa M, la Fougère C, Hampel H (2010) Functional representation of olfactory impairment in early Alzheimer's disease. J Alzheimer's Dis 22(2):581–591. https://doi.org/10.3233/JAD-2010-091549

Fox NC, Warrington EK, Freeborough PA, Hartikainen P, Kennedy AM, Stevens JM, Rossor MN (1996) Presymptomatic hippocampal atrophy in Alzheimer's disease: a longitudinal MRI study. Brain 119(6):2001–2007. https://doi.org/10.1093/brain/119.6.2001

Giaccio RG (2006) The dual origin hypothesis: An evolutionary brain-behavior framework for analyzing psychiatric disorders. Neurosci Biobehav Rev 30(4):526–550. https://doi.org/10.1016/j.neubiorev.2005.04.021

Golebiowski M, Barcikowska M, Pfeffer A (1999) Magnetic resonance imaging-based hippocampal volumetry in patients with dementia of the Alzheimer type. Dement Geriatr Cogn Disord 10(4):284–288. https://doi.org/10.1159/000017133

Grober E, Sanders AE, Hall C, Lipton RB (2010) Free and cued selective reminding identifies very mild dementia in primary care. Alzheimer Dis Assoc Disord 24(3):284–290. https://doi.org/10.1097/WAD.0b013e3181cfc78b

Herzog AG, Kemper TL (1980) Amygdaloid changes in aging and dementia. Arch Neurol 37(10):625–629. https://doi.org/10.1001/archneur.1980.00500590049006

Heun R, Mazanek M, Atzor K-R, Tintera J, Gawehn J, Burkart M, Stoeter P (1997) Amygdala-hippocampal atrophy and memory performance in dementia of Alzheimer type. Dementia Geriatric Cognit Disord 8(6):329–336. https://doi.org/10.1159/000106651

Horínek D, Varjassyová A, Hort J (2007) Magnetic resonance analysis of amygdalar volume in Alzheimer's disease. Curr Opin Psychiatry 20(3):273–277. https://doi.org/10.1097/YCO.0b013e3280ebb613

Iglesias JE, Augustinack JC, Nguyen K, Player CM, Player A, Wright M, Van Leemput K (2015) A computational atlas of the hippocampal formation using ex vivo, ultra-high resolution MRI: application to adaptive segmentation of in vivo MRI. Neuroimage 115:117–137. https://doi.org/10.1016/j.neuroimage.2015.04.042

Insel PS, Young CB, Johnson KA, Sperling RA, Mormino EC, Donohue MC (2023) Tau positron emission tomography in preclinical Alzheimer's disease. Brain 146(2):700–711. https://doi.org/10.1093/brain/awac299

Ivnik RJ, Smith GE, Lucas JA, Tangalos EG, Kokmen E, Petersen RC (1997) Free and cued selective reminding test: MOANS norms. J Clin Exp Neuropsychol 19(5):676–691. https://doi.org/10.1080/01688639708403753

Jack CRJ, Knopman DS, Jagust WJ, Shaw LM, Aisen PS, Weiner MW, Trojanowski JQ (2010) Hypothetical model of dynamic biomarkers of the Alzheimer's pathological cascade. Lancet Neurol 9(1):119–128. https://doi.org/10.1016/S1474-4422(09)70299-6

Jack CR, Barkhof F, Bernstein MA, Cantillon M, Cole PE, DeCarli C, Frisoni GB (2011) Steps to standardization and validation of hippocampal volumetry as a biomarker in clinical trials and diagnostic criterion for Alzheimer's disease. Alzheimer Dementia 7(4):474–485. https://doi.org/10.1016/j.jalz.2011.04.007

Jessen F, Wolfsgruber S, Wiese B, Bickel H, Mösch E, Kaduszkiewicz H, Wagner M (2014) AD dementia risk in late MCI, in early MCI, and in subjective memory impairment Alzheimer's & Dementia. J Alzheimer's Assoc 10(1):76–83. https://doi.org/10.1016/j.jalz.2012.09.017

Kotecha AM, Corrêa ADC, Fisher KM, Rushworth JV (2018) Olfactory dysfunction as a global biomarker for sniffing out Alzheimer's disease: a meta-analysis. Biosensors 8(2):41. https://doi.org/10.3390/bios8020041

Lehmann M, Douiri A, Kim LG, Modat M, Chan D, Ourselin S, Fox NC (2010) Atrophy patterns in Alzheimer's disease and semantic dementia: a comparison of FreeSurfer and manual volumetric measurements. Neuroimage 49(3):2264–2274. https://doi.org/10.1016/j.neuroimage.2009.10.056

Liu Y, Paajanen T, Zhang Y, Westman E, Wahlund L-O, Simmons A, Tsolaki M (2010) Analysis of regional MRI volumes and thicknesses as predictors of conversion from mild cognitive impairment to Alzheimer's disease. Neurobiol Aging 31(8):1375–1385. https://doi.org/10.1016/j.neurobiolaging.2010.01.022

Lockhart SN, Schöll M, Baker SL, Ayakta N, Swinnerton KN, Bell RK, Janabi M (2017) Amyloid and tau PET demonstrate region-specific associations in normal older people. Neuroimage 150:191–199. https://doi.org/10.1016/j.neuroimage.2017.02.051

Mai JK, Paxinos G (2011) The human nervous system. Academic Press. https://doi.org/10.1016/C2009-0-02721-4

McKhann GM, Knopman DS, Chertkow H, Hyman BT, Jack CRJ, Kawas CH, Phelps CH (2011) The diagnosis of dementia due to Alzheimer's disease: recommendations from the National Institute on Aging-Alzheimer's Association workgroups on diagnostic guidelines for Alzheimer's disease Alzheimer's & dementia. J Alzheimer's Assoc 7(3):263–269. https://doi.org/10.1016/j.jalz.2011.03.005

Molinuevo JL, Rabin LA, Amariglio R, Buckley R, Dubois B, Ellis KA, Group, S. C. D. I. (SCD-I. W) (2017) Implementation of subjective cognitive decline criteria in research studies Alzheimer's and dementia. J Alzheimer's Assoc 13(3):296–311. https://doi.org/10.1016/j.jalz.2016.09.012

Morris JC (1991) The clinical dementia rating (cdr): current version and. Young 41:1588–1592. https://doi.org/10.1212/WNL.43.11.2412-a

Pandya D, Petrides M, Cipolloni PB (2015) Cerebral cortex: architecture, connections, and the dual origin concept. Oxford University Press. https://doi.org/10.1093/med/9780195385151.001.0001

Petersen RC (2004) Mild cognitive impairment as a diagnostic entity. J Intern Med 256(3):183–194. https://doi.org/10.1111/j.1365-2796.2004.01388.x

Poulin SP, Dautoff R, Morris JC, Barrett LF, Dickerson BC, Initiative ADN (2011) Amygdala atrophy is prominent in early Alzheimer's disease and relates to symptom severity. Psychiatry Res Neuroimaging 194(1):7–13. https://doi.org/10.1016/j.pscychresns.2011.06.014

Price JL, Morris JC (1999) Tangles and plaques in nondemented aging and "preclinical" Alzheimer's disease. Ann Neurol 45(3):358–368. https://doi.org/10.1002/1531-8249(199903)45:3%3c358::AID-ANA12%3e3.0.CO;2-X

Price JL, Davis PB, Morris JC, White DL (1991) The distribution of tangles, plaques and related immunohistochemical markers in healthy aging and Alzheimer's disease. Neurobiol Aging 12(4):295–312. https://doi.org/10.1016/0197-4580(91)90006-6

Quarmley M, Moberg PJ, Mechanic-Hamilton D, Kabadi S, Arnold SE, Wolk DA, Roalf DR (2017) Odor identification screening improves diagnostic classification in incipient Alzheimer's disease. J Alzheimer's Dis 55(4):1497–1507. https://doi.org/10.3233/JAD-160842

Roberts RO, Geda YE, Knopman DS, Cha RH, Pankratz VS, Boeve BF, Rocca WA (2008) The mayo clinic study of aging: design and sampling, participation, baseline measures and sample characteristics. Neuroepidemiology 30(1):58–69. https://doi.org/10.1159/000115751

Sanabria-Castro A, Alvarado-Echeverría I, Monge-Bonilla C (2017) Molecular pathogenesis of Alzheimer's disease: an update. Ann Neurosci 24(1):46–54. https://doi.org/10.1159/000464422

Saygin ZM, Kliemann D, Iglesias JE, van der Kouwe AJW, Boyd E, Reuter M, Frosch MP (2017) High-resolution magnetic resonance imaging reveals nuclei of the human amygdala: manual segmentation to automatic atlas. Neuroimage 155:370–382. https://doi.org/10.1016/j.neuroimage.2017.04.046

Scheltens P, Leys D, Barkhof F, Huglo D, Weinstein HC, Vermersch P, Valk J (1992) Atrophy of medial temporal lobes on MRI in "probable" Alzheimer's disease and normal ageing: diagnostic value and neuropsychological correlates. J Neurol Neurosurg Psychiatry 55(10):967–972. https://doi.org/10.1136/jnnp.55.10.967

Schöll M, Lockhart SN, Schonhaut DR, O'Neil JP, Janabi M, Ossenkoppele R, Schwimmer HD (2016) PET imaging of tau deposition in the aging human brain. Neuron 89(5):971–982. https://doi.org/10.1016/j.neuron.2016.01.028

Schultz C, Engelhardt M (2014) Anatomy of the hippocampal formation. Front Neurol Neurosci 34:6–17. https://doi.org/10.1159/000360925

Scott SA, Sparks DL, Scheff SW, Dekosky ST, Knox CA (1992) Amygdala cell loss and atrophy in Alzheimer's disease. Ann Neurol 32(4):555–563. https://doi.org/10.1002/ana.410320412

Seligman SC, Kamath V, Giovannetti T, Arnold SE, Moberg PJ (2013) Olfaction and apathy in Alzheimer's disease, mild cognitive impairment, and healthy older adults. Aging Ment Health 17(5):564–570. https://doi.org/10.1080/13607863.2013.768208

Small SA, Schobel SA, Buxton RB, Witter MP, Barnes CA (2011) A pathophysiological framework of hippocampal dysfunction in ageing and disease. Nat Rev Neurosci 12(10):585–601. https://doi.org/10.1038/nrn3085

Sperling RA, Mormino EC, Schultz AP, Betensky RA, Papp KV, Amariglio RE, Hedden T (2019) The impact of amyloid-beta and tau on prospective cognitive decline in older individuals. Ann Neurol 85(2):181–193. https://doi.org/10.1002/ana.25395

Squire LR, Stark CEL, Clark RE (2004) The medial temporal lobe. Annu Rev Neurosci 27:279–306. https://doi.org/10.1146/annurev.neuro.27.070203.144130

van Strien NM, Cappaert NLM, Witter MP (2009) The anatomy of memory: an interactive overview of the parahippocampal-hippocampal network. Nat Rev Neurosci 10(4):272–282. https://doi.org/10.1038/nrn2614

Velayudhan L, Gasper A, Pritchard M, Baillon S, Messer C, Proitsi P (2015) Pattern of smell identification impairment in Alzheimer's disease. J Alzheimer's Dis 46(2):381–387. https://doi.org/10.3233/JAD-142838

Vemuri P, Lowe VJ, Knopman DS, Senjem ML, Kemp BJ, Schwarz CG, Jack CR Jr (2017) Tau-PET uptake: regional variation in average SUVR and impact of amyloid deposition. Alzheimer's Dement 6:21–30. https://doi.org/10.1016/j.dadm.2016.12.010

Vogt LJK, Hyman BT, Van Hoesen GW, Damasio AR (1990) Pathological alterations in the amygdala in Alzheimer's disease. Neuroscience 37(2):377–385. https://doi.org/10.1016/0306-4522(90)90408-V

Wang J, Eslinger PJ, Doty RL, Zimmerman EK, Grunfeld R, Sun X, Smith MB (2010) Olfactory deficit detected by fMRI in early Alzheimer's disease. Brain Res 1357:184–194. https://doi.org/10.1016/j.brainres.2010.08.018

Ward AM, Calamia M, Thiemann E, Dunlap J, Tranel D (2017) Association between olfaction and higher cortical functions in Alzheimer's disease, mild cognitive impairment, and healthy older adults. J Clin Exp Neuropsychol 39(7):646–658. https://doi.org/10.1080/13803395.2016.1253667

Wilson RS, Li Y, Aggarwal NT, McCann JJ, Gilley DW, Bienias JL, Evans DA (2006) Cognitive decline and survival in Alzheimer's disease. Int J Geriatr Psychiatry 21(4):356–362. https://doi.org/10.1002/gps.1472

Wolk DA, Das SR, Mueller SG, Weiner MW, Yushkevich PA, Initiative ADN (2017) Medial temporal lobe subregional morphometry using high resolution MRI in Alzheimer's disease. Neurobiol Aging 49:204–213. https://doi.org/10.1016/j.neurobiolaging.2016.09.011

Yilmazer-Hanke DM (2012) Amygdala. In: Mai JK (ed) Third E. Paxinos. Academic Press, San Diego, pp 759–834. https://doi.org/10.1016/B978-0-12-374236-0.10022-7

Yushkevich PA, Pluta JB, Wang H, Xie L, Ding S, Gertje EC, Wolk DA (2015) Automated volumetry and regional thickness analysis of hippocampal subfields and medial temporal cortical structures in mild cognitive impairment. Hum Brain Mapp 36(1):258–287. https://doi.org/10.1002/hbm.22627

Yushkevich PA, Muñoz López M, de Onzoño I, Martin MM, Ittyerah R, Lim S, Ravikumar S, Wang J (2021) Three-dimensional mapping of neurofibrillary tangle burden in the human medial temporal lobe. Brain 144(9):2784–2797. https://doi.org/10.1093/brain/awab262

Publisher's Note Springer Nature remains neutral with regard to jurisdictional claims in published maps and institutional affiliations.

Springer Nature or its licensor (e.g. a society or other partner) holds exclusive rights to this article under a publishing agreement with the author(s) or other rightsholder(s); author self-archiving of the accepted manuscript version of this article is solely governed by the terms of such publishing agreement and applicable law.